Amino Acids (2011) 41:1059–1070
DOI 10.1007/s00726-009-0439-0

ORIGINAL ARTICLE

Impact of bifunctional chelators on biological properties of ^{111}In-labeled cyclic peptide RGD dimers

Jiyun Shi · Young-Seung Kim · Sudipta Chakraborty · Yang Zhou · Fan Wang · Shuang Liu

Received: 17 September 2009 / Accepted: 28 November 2009 / Published online: 6 January 2010

Abstract The present study describes the synthesis and biological evaluation of ^{111}In(DOTA-3P-RGD$_2$) (DOTA = 1,4,7,10-tetraazacyclo-dodecane-1,4,7,10-tetraacetic acid; 3P-RGD$_2$ = PEG$_4$-E[PEG$_4$-c(RGDfK)]$_2$; PEG$_4$ = 15-amino-4,7,10,13-tetraoxapentadecanoic acid), ^{111}In(DTPA-3P-RGD$_2$) (DTPA = diethylenetriaminepentaacetic acid) and ^{111}In(DTPA-Bn-3P-RGD$_2$) (DTPA-Bn = 2-(*p*-thioureidobenzyl)-diethylenetriaminepentaacetic acid) as potential radiotracers for imaging tumor integrin $\alpha_v\beta_3$ expression in athymic nude mice bearing U87MG glioma xenografts. The aim of the study is to assess the impact of the bifunctional chelator (BFC) (DOTA vs. DTPA or DTPA-Bn) on the biodistribution characteristics of the ^{111}In-labeled 3P-RGD$_2$. IC$_{50}$ values of DOTA-3P-RGD$_2$, DTPA-3P-RGD$_2$ and DTPA-Bn-3P-RGD$_2$ were determined to be 1.3 ± 0.2, 1.4 ± 0.3, 1.3 ± 0.3 nM, respectively, against ^{125}I-c(RGDyK) bound to U87MG human glioma cells. Radiotracers were prepared by reacting ^{111}InCl$_3$ with the RGD peptide conjugates in NH$_4$OAc buffer (100 mM, pH 5.5). For DOTA-3P-RGD$_2$, successful radiolabeling could be completed by heating the reaction mixture at 100°C for 15–20 min. For DTPA-3P-RGD$_2$ and DTPA-Bn-3P-RGD$_2$, the radiolabeling was almost instantaneous at room temperature. The specific activity was ~50 mCi/mg (or ~100 mCi/μmol) for ^{111}In(DOTA-3P-RGD$_2$) and ~200 mCi/mg (or ~400 mCi/μmol) for ^{111}In(DTPA-3P-RGD$_2$). The results from biodistribution studies showed that all the three radiotracers have high tumor uptake and excellent tumor-to-background (T/B) ratios up to 4-h postinjection. After that time point, both ^{111}In(DTPA-3P-RGD$_2$) and ^{111}In(DTPA-Bn-3P-RGD$_2$) showed a much faster tumor washout and poorer T/B ratios than ^{111}In(DOTA-3P-RGD$_2$). The tumor uptake of ^{111}In(DOTA-3P-RGD$_2$) is integrin $\alpha_v\beta_3$- and RGD-specific. ^{111}In(DOTA-3P-RGD$_2$) is metabolically stable while only ~25% of ^{111}In(DTPA-Bn-3P-RGD$_2$) remains intact in the feces during 2-h period. On the basis of results from this study, it was concluded that ^{111}In(DTPA-3P-RGD$_2$) can be an effective integrin $\alpha_v\beta_3$-targeted radiotracer if the high-specific activity is required. However, DOTA remains to be the BFC of choice for the development of therapeutic lanthanide radiotracers.

Keywords Integrin $\alpha_v\beta_3$ · ^{111}In-labeled cyclic RGD peptides · Tumor imaging

J. Shi · Y.-S. Kim · S. Chakraborty · Y. Zhou · S. Liu (✉)
School of Health Sciences, Purdue University,
550 Stadium Mall Drive, West Lafayette, IN 47907, USA
e-mail: lius@pharmacy.purdue.edu; liu100@purdue.edu

J. Shi · F. Wang
Medical Isotopes Research Center,
Peking University, 100083 Beijing, China

Introduction

Over last several years, many radiolabeled cyclic RGD peptides have been evaluated for imaging integrin $\alpha_v\beta_3$-positive tumors by single photon emission computed tomography (SPECT) or positron emission tomography (PET) (Haubner et al. 1999; Weber et al. 2001; Liu et al. 2001b, 2003, 2007; Janssen et al. 2002; Thumshirn et al. 2003, Chen et al. 2004a, c, d; Beer et al. 2005; Wu et al. 2005, 2007a, b; Chen 2006; Liu 2006; Decristoforo et al. 2006, Jia et al. 2006, 2008; Dijkgraaf et al. 2007a, b; Kenny et al. 2008). Multimeric cyclic RGD peptides, such as E[c(RGDfK)]$_2$ (RGD$_2$) and E{E[c(RGDfK)]$_2$}$_2$ (RGD$_4$), have been successfully used to improve the integrin $\alpha_v\beta_3$-binding affinity and radiotracer tumor uptake (Janssen et al.

2002; Thumshirn et al. 2003; Chen et al. 2004a, d; Wu et al. 2005, 2007a, b; Liu 2006; Jia et al. 2006, 2008; Dijkgraaf et al. 2007a, b; Liu et al. 2007). It has been demonstrated that the radiolabeled (^{99m}Tc, ^{111}In, ^{18}F and ^{64}Cu) multimeric cyclic RGD peptides, such as RGD_2 and RGD_4, have much better tumor targeting capability as evidenced by their higher integrin $\alpha_v\beta_3$-binding affinity, better tumor uptake and longer tumor retention time than their corresponding monomeric counterparts (Janssen et al. 2002; Thumshirn et al. 2003; Chen et al. 2004a, d; Wu et al. 2005, 2007a, b; Liu 2006; Jia et al. 2006, 2008; Dijkgraaf et al. 2007a, b; Liu et al. 2007). Recently, we reported [^{99m}Tc(HYNIC-3P-RGD_2)(tricine)(TPPTS)] (^{99m}Tc-3P-RGD_2: HYNIC = 6-hydrazinonicotinyl; 3P-RGD_2 = PEG_4-E[PEG_4-c(RGDfK)]$_2$; PEG_4 = 15-amino-4,7,10,13-tetraoxapentadecanoic acid; and TPPTS = trisodium triphenylphosphine-3,3′,3″-trisulfonate) and [^{99m}Tc(HYNIC-3G-RGD_2)(tricine)(TPPTS)] (^{99m}Tc-3G-RGD_2: 3G-RGD_2 = G_3-E[G_3-c(RGDfK)]$_2$; and G_3 = Gly-Gly-Gly) as SPECT radiotracers for imaging tumors in athymic nude mice bearing U87MG glioma and MDA-MB-435 breast cancer xenografts (Shi et al. 2008; Wang et al. 2009). It was found that the PEG_4 and G_3 linkers are useful for enhancing the integrin $\alpha_v\beta_3$ targeting capability of cyclic RGD peptide dimers via simultaneous integrin $\alpha_v\beta_3$ binding of the two cyclic RGD motifs. Similar results were also obtained for ^{64}Cu(DOTA-3P-RGD_2) (DOTA = 1,4,7,10-tetraazacyclododecane-1,4,7,10-tetraacetic acid) and ^{64}Cu(DOTA-3G-RGD_2) (Shi et al. 2009).

In this report, we now present the evaluation of ^{111}In(DOTA-3P-RGD_2), ^{111}In(DTPA-3P-RGD_2) (DTPA = diethylenetriaminepentaacetic acid), and ^{111}In(DTPA-Bn-3P-RGD_2) (DTPA-Bn = 2-(*p*-thioureidobenzyl)diethylenetriaminepentaacetic acid) (Fig. 1) as integrin $\alpha_v\beta_3$-targeted radiotracers. ^{111}In has two gamma emissions with the photon energy of 173 and 247 keV (90 and 95% abundance, respectively), and has been widely used (only second to ^{99m}Tc) in gamma scintigraphy or SPECT. The ^{111}In-labeled biomolecules are also useful as imaging surrogates for dosimetry calculations of their corresponding ^{90}Y analogs for radiotherapy of cancer. DOTA was used as the bifunctional chelator (BFC) since it has been successfully used for ^{64}Cu, ^{68}Ga, ^{90}Y, ^{177}Lu and ^{111}In-labeling of peptides and small biomolecules (Heppeler et al. 1999; Liu and Edwards 2001a; Kowalski et al. 2003; Bodei et al. 2004; Chen et al. 2004b; McQuade et al. 2005; Koukouraki et al. 2006; Kwekkeboom et al. 2008; Liu 2008). The disadvantage of using DOTA as the BFC is its slow chelation kinetics and low radiolabeling efficiency (Liu and Edwards 2001a; Liu et al. 2001a; Jia et al. 2008; Liu 2008). In contrast, DTPA and its derivatives have much higher radiolabeling efficiency (fast and high labeling yield) (Stimmel and Kull 1998; Liu and Edwards 2001a, b; Jia et al. 2008; Liu 2008). As a result, the resulting ^{111}In-labeled small biomolecules have significantly high-specific activity (Bakker et al. 1991; Liu and Edwards 2001b; de Visser et al. 2007; Jia et al. 2008). The main objective of this study is to determine if ^{111}In(DTPA-3P-RGD_2) can be an effective integrin $\alpha_v\beta_3$-targeted radiotracer and explore the impact of BFCs (DOTA vs. DTPA and DTPA-Bn) on tumor uptake and tumor-to-background (T/B) ratios of the ^{111}In-labeled 3P-RGD_2.

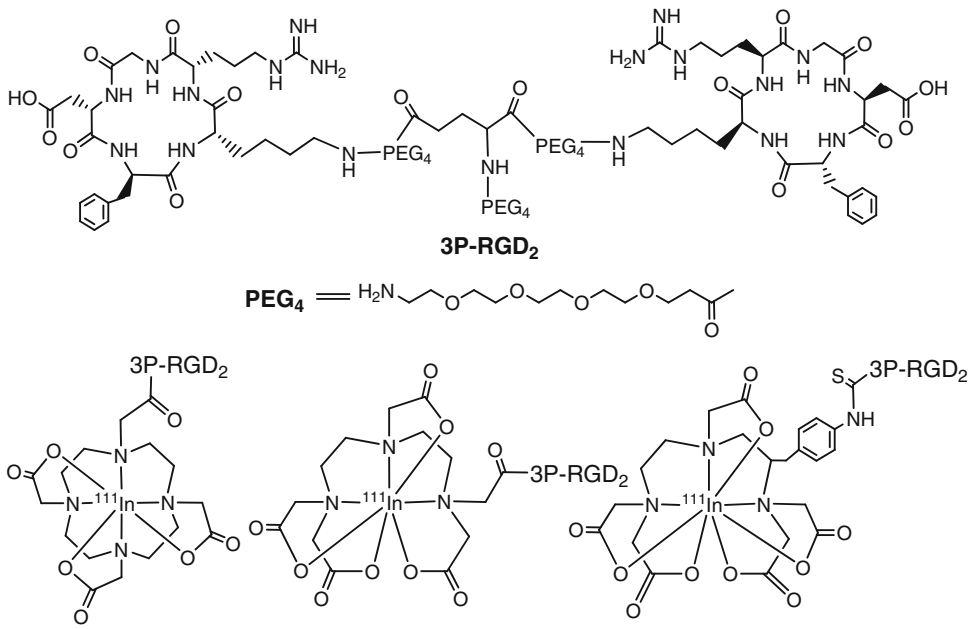

Fig. 1 ^{111}In-labeled 3P-RGD_2: ^{111}In(DOTA-3P-RGD_2), ^{111}In(DTPA-3P-RGD_2) and ^{111}In(DTPA-Bn-3P-RGD_2)

Experimental

Materials and methods

Chemicals were purchased from Sigma/Aldrich (St. Louis, MO) unless otherwise mentioned, and were used without further purification. PEG_4-E[PEG_4-c(RGDfK)]$_2$ (3P-RGD_2) and PEG_4-E[PEG_4-c(RGKfD)]$_2$ (3P-RGK_2: a scrambled nonsense peptide) were obtained from the Peptides International Inc. (Louisville, KY). DO3A-OSu [1,4,7, 10-tetraazacyclododecane-4,7,10-triacetic acid-1-acetate (*N*-hydroxysuccinamide)] and *p*-SCN-Bn-DTPA (2-(*p*-isothiocyanobenzyl)-diethylenetriaminepentaacetic acid) were purchased from Macrocyclics (Dallas, TX). $^{111}InCl_3$ was obtained from Perkin-Elmer Life and Analytical Sciences (North Billerica, MA). DOTA-3P-RGD_2 was prepared according to the literature procedures (Shi et al. 2009). The NH_4OAc buffer for ^{111}In-labeling studies was passed over a Chelex-100 column (1 cm × 15 cm) to minimize the trace metal contaminants. The semi-preparative HPLC Method 1 and 2 used a LabAlliance HPLC system equipped with a UV/vis detector ($\lambda = 254$ nm) and Zorbax C_{18} semi-prep column (9.4 mm × 250 mm, 100 Å pore size, Agilent Technologies, Santa Clara, CA). Method 1: the mobile phase starting from 90% solvent A (0.1% TFA in water) and 10% solvent B (0.1% TFA in acetonitrile) at 0 min, followed by a gradient mobile phase going from 85% A and 15% B at 5 min to 50% solvent A and 50% solvent B at 25 min. Method 2: the mobile phase being isocratic with 80% solvent A and 20% solvent B at 0-5 min, followed by a gradient mobile phase going from 20% solvent B at 5 min to 50% solvent B at 10–15 min and back to 20% solvent B at 20 min. The radio-HPLC method (Method 3) used the LabAlliance HPLC system equipped with a *β*-ram IN/US detector (Tampa, FL) and Zorbax C_{18} column (4.6 mm × 250 mm, 300 Å pore size; Agilent Technologies, Santa Clara, CA). The flow rate was 1 mL/min. The mobile phase was isocratic with 90% A (25 mM NH_4OAc, pH 6.8) and 10% B (acetonitrile) at 0–5 min, followed by a gradient mobile phase going from 10% solvent B at 5 min to 15% solvent B at 15 min and to 50% solvent B at 20–25 min, then back to an isocratic mobile phase with 10% CH_3CN at 26–32 min.

DTPA-3P-RGD_2

DTPA dianhydride (2.9 mg, ~8.1 μM) and 3P-RGD_2 (4.4 mg, ~2.1 μM) were dissolved in a mixture of 1.5 mL of anhydrous DMF and 0.5 mL of DMSO. The pH in the reaction mixture was adjusted to 8.5–9.0 with DIEA. The reaction mixture was stirred overnight at room temperature. After addition of 3 mL of 100 mM NH_4OAc buffer (pH 7.0), the resulting solution was filtered, and the filtrate was subjected to HPLC-purification (Method 1). The fraction at ~16.4 min was collected. Lyophilization of the collected fractions afforded the expected product DTPA-3P-RGD_2. The yield was 1.9 mg (~37%). ESI–MS (positive mode) for DTPA-3P-RGD_2: *m/z* 2,434.38 for $[M+H]^+$ (*M* 2,434.2 calcd. for $C_{106}H_{171}N_{25}O_{40}$) and 1,218.42 for $[M+2H]^{2+}$.

DTPA-Bn-3P-RGD_2

DTPA-Bn-SCN (4.1 mg, ~7.6 μM) and 3P-RGD_2 (3.6 mg, ~1.8 μM) were dissolved in 1 mL of DMF. The pH in the reaction mixture was adjusted to 8.5–9.0 with DIEA. The reaction mixture was stirred overnight at room temperature. After addition of 3 mL of 100 mM NH_4OAc buffer (pH 7.0), the resulting solution was filtered to remove any precipitate, and the filtrate was subjected to HPLC-purification (Method 2). The fraction at ~12.8 min was collected. Lyophilization of the collected fractions afforded the product DTPA-Bn-3P-RGD_2. The yield was 2.0 mg (~43%). ESI–MS (positive mode) for DTPA-Bn-3P-RGD_2: *m/z* 2,622.72 for $[M+Na]^+$ (*M* 2,600.24 calcd. for $C_{114}H_{178}N_{26}O_{41}S$) and 1,301.01 for $[M+2H]^{2+}$.

DOTA-3P-RGK_2

DOTA-OSu (5.0 mg, ~10.0 μmol) and 3P-RGK_2 (10.30 mg, ~5.0 μmol) were dissolved in DMF (1 mL). After addition of DIEA (2 drops), the reaction mixture was stirred at room temperature for 2 h. The reaction was terminated by addition of 3 mL NH_4OAc buffer (100 mM, pH 7.0). The product was separated from the mixture by HPLC (Method 1). The fraction at ~17.5 min was collected. Lyophilization of collected fractions afforded DOTA-3P-RGK_2 with 95% purity. The yield was 4.0 mg (~33%). ESI–MS (positive mode): *m/z* 2,447.35 for $[M+H]^+$ (*M* 2,446 calcd. for $[C_{108}H_{176}N_{26}O_{38}]^+$).

^{111}In-labeling and dose preparation

For the preparation of ^{111}In(DOTA-3P-RGD_2) and ^{111}In(DOTA-3P-RGK_2), to a clean Eppendorf tube were added 200 μL of DOTA conjugate solution (1.0 mg/mL in 0.2 M NH_4OAc buffer, pH 5.5) and 50 μL of $^{111}InCl_3$ solution (~500 μCi in 0.05 M HCl). The vial was heated at 100°C for ~15 min in a lead-shielded water bath. After heating, the Eppendorf tube was placed back into the lead pig, and allowed to stand at room temperature for ~10 min. ^{111}In(DTPA-3P-RGD_2) and ^{111}In(DTPA-Bn-3P-RGD_2) were prepared in similar fashion except that the reaction mixture was kept at room temperature for 15–20 min. A sample of the resulting solution was analyzed by the radio-HPLC (Method 3). The radiochemical

purity (RCP) was >95% for all new ^{111}In radiotracers. The water–octanol partition coefficients of new ^{111}In radiotracers were determined according to the literature methods (Jia et al. 2008; Shi et al. 2008, 2009; Wang et al. 2009). The log *P* values were measured three different times, and were reported as an average of three independent measurements plus the standard deviation. For biodistribution studies, the ^{111}In radiotracers were purified by HPLC (Method 3). Volatiles in the HPLC mobile phase were removed under vacuum ($\sim$5 mmHg) at room temperature. Doses were prepared by dissolving the purified radiotracer in saline to 70–100 μCi/mL. For planar imaging studies, doses were prepared by dissolving the radiotracer in saline to $\sim$1 mCi/mL. For the blocking experiment, RGD_2 was dissolved in the radiotracer solution to give a concentration of 3.5 mg/mL. The resulting solution was filtered with a 0.20 μm Millex-LG filter before being injected into animals. Each animal was injected with 0.1–0.2 mL of the dose solution.

In vitro whole-cell integrin $\alpha_v\beta_3$-binding assay

The integrin-binding affinity of RGD peptides was assessed via a displacement assay using ^{125}I-c(RGDyK) as the integrin-specific radioligand. Briefly, U87MG glioma cells were grown in Minimum Essential Medium (MEM) supplemented with 10% fetal bovine serum (FBS), 100 IU/ml penicillin and 100 μg/ml streptomycin (Invitrogen Co, Carlsbad, CA), at 37°C in humidified atmosphere containing 5% CO_2. Filter multiscreen DV plates were seeded with 10^5 glioma cells in binding buffer and incubated with ^{125}I-c(RGDyK) in the presence of increasing concentrations of the RGD peptides. After removing the unbound ^{125}I-c(RGDyK), hydrophilic PVDF filters were collected and the radioactivity was determined using a gamma counter (Packard, Meriden, CT). The IC_{50} values were calculated by fitting the data by nonlinear regression using GraphPad Prism™ (GraphPad Software Inc., San Diego, CA). Experiments were carried out twice with triplicate samples. The IC_{50} values are reported as an average of these samples plus the standard deviation.

Animal model

Biodistribution and imaging studies were performed using athymic nude mice bearing U87MG human glioma xenografts in compliance with NIH animal experiment guidelines (Principles of Laboratory Animal Care, NIH Publication No. 86-23, revised 1985). The animal protocol was approved by the Purdue University Animal Care and Use Committee (PACUC). U87MG glioma cells were cultured in the Minimum Essential Medium, Eagle with Earle's Balanced Salt Solution (non-essential amino acids sodium pyruvate) (ATCC, Manassas, VA) in humidified atmosphere of 5% carbon dioxide. 10% FBS (Sigma, St. Louis, MO) and 1% Penicillin/Streptomycin (GIBCO, Grand Island, NY) were added into the medium. Female athymic nu/nu mice were purchased from Harlan (Indianapolis, IN) at 4–5 weeks of age. Each mouse was implanted subcutaneously with 5×10^6 tumor cells into the left and right upper flanks. In this way, one could assess the impact of tumor size on the radiotracer imaging quality in a single tumor-bearing mouse. All procedures were performed in a laminar flow cabinet using aseptic technique. Three weeks after inoculation, the tumor size was 0.1–0.4 g, and animals were used for biodistribution and imaging studies.

Biodistribution protocol

Twenty tumor-bearing mice (20–25 g) were randomly divided into four groups. Each animal was administered with 2–5 μCi of ^{111}In radiotracer by tail vein injection. Four animals were killed by sodium pentobarbital overdose ($\sim$200 mg/kg) at 0.5, 1, 4, 24 and 72 h postinjection (p.i.). Blood samples were withdrawn from the heart. The tumor and normal organs (brain, eyes, heart, spleen, lungs, liver, kidneys, muscle and intestine) were excised, washed with saline, dried with absorbent tissue, weighed, and counted on a Perkin Elmer Wizard—1480 γ-counter (Shelton, CT). The organ uptake was calculated as the percentage of injected dose per gram of organ mass (%ID/g) or the percentage of injected dose per organ (%ID/organ).

Planar imaging

The imaging study was performed by using the athymic nude mice ($n = 3$) bearing U87MG human glioma xenografts. Each tumor-bearing mouse was administered with $\sim$100 μCi of ^{111}In(DOTA-3P-RGD_2) or ^{111}In(DTPA-3P-RGD_2). Animals were anesthetized with intraperitoneal injection of ketamine (80 mg/kg) and xylazine (19 mg/kg), and then were placed supine on a single head mini γ-camera (Diagnostic Services Inc., NJ) equipped with a medium-energy collimator. Anterior images were acquired at 1, 4, 24 and 72 h p.i. The imaging data were stored digitally in a 128×128 matrix. The acquisition count limits were set at 300 K. After completion of imaging, animals were killed by sodium pentobarbital overdose ($\sim$200 mg/kg).

Metabolism

Normal athymic nude mice ($n = 2$) were used for metabolism studies. Each mouse was administered with $\sim$100 μCi of ^{111}In(DOTA-3P-RGD_2) or ^{111}In(DTPA-Bn-3P-RGD_2).

The urine samples were collected at 30 and 120 min p.i. by manual void, and were mixed with equal volume of 20% acetonitrile aqueous solution. The mixture was centrifuged at 8,000 rpm. The supernatant was collected and passed through a 0.20 μm Millex-LG filter unit to remove any precipitate or foreign particles. The filtrate was analyzed by radio-HPLC (Method 3). Feces samples were collected at 2 h p.i. and suspended in 20% acetonitrile aqueous solution. The resulting mixture was vortexed for 5–10 min. After centrifuging at 8,000 rpm, the supernatant was collected and passed through a 0.20 μm Millex-LG filter unit to remove any precipitate or foreign particles. The filtrate was analyzed by radio-HPLC (Method 3). The radioactivity recovery was >95% (by γ-counting) for both urine and feces samples.

Data and statistical analysis

The biodistribution data and target-to-background (T/B) ratios are reported as an average plus the standard variation based on results from four tumor-bearing mice at each time point. Comparison between two different radiotracers was made using the two-way ANOVA test (GraphPad Prim 5.0, San Diego, CA). The level of significance was set at $P < 0.05$.

Results

Synthesis of DTPA and DOTA conjugates

DTPA-3P-RGD$_2$ and DTPA-Bn-3P-RGD$_2$ were prepared by direct conjugation of 3P-RGD$_2$ with excess DTPA bis-anhydride and *p*-SCN-Bn-DTPA, respectively. DOTA-3P-RGK$_2$ was prepared by reacting 3P-RGK$_2$ with DOTA-OSu in DMF in the presence of excess DIEA. DOTA-3P-RGK$_2$ has the same number of amino acid residues as that in DOTA-3P-RGD$_2$; but the peptide sequence is "scrambled" using c(RGKfD) instead of c(RGDfK). It was designed to demonstrate the RGD-specificity of ^{111}In(DOTA-3P-RGD$_2$). DTPA-3P-RGD$_2$, DTPA-Bn-3P-RGD$_2$ and DOTA-3P-RGK$_2$ were all purified by HPLC. The HPLC purity was >95% before being used for ^{111}In-labeling and determination of their integrin $\alpha_v\beta_3$-binding affinity.

Integrin $\alpha_v\beta_3$-binding affinity

Figure 2 shows displacement curves of c(RGDyK), DOTA-3P-RGD$_2$, DTPA-3P-RGD$_2$, DTPA-Bn-3P-RGD$_2$ and DOTA-3P-RGK$_2$ against ^{125}I-c(RGDyK) bound to the U87MG glioma cells. c(RGDyK) was evaluated in the same assay for comparison purposes. Their IC$_{50}$ values were calculated to be 49.9 ± 5.5, 1.3 ± 0.2, 1.4 ± 0.3, 1.3 ± 0.3 and 715.8 ± 45.1 nM, respectively.

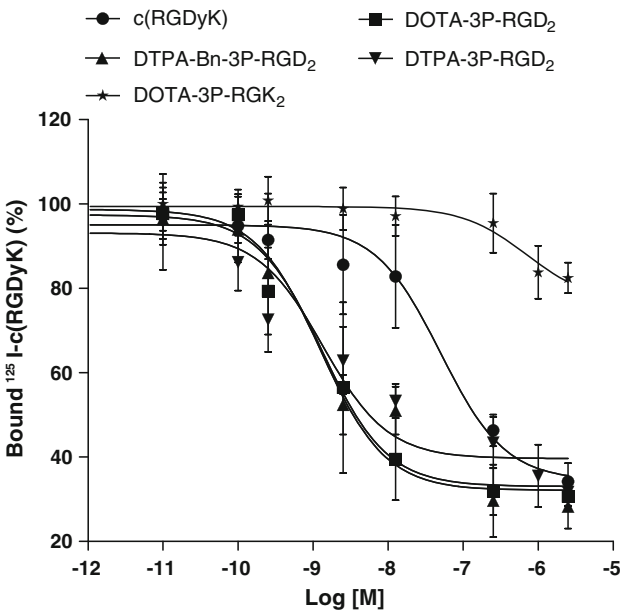

Fig. 2 In vitro competitive inhibition of ^{125}I-c(RGDyK) bound to the integrin $\alpha_v\beta_3$-positive U87MG human glioma cells by c(RGDyK), DOTA-3P-RGD$_2$, DTPA-3P-RGD$_2$, DTPA-Bn-3P-RGD$_2$ and DOTA-3P-RGK$_2$. Their IC$_{50}$ values were calculated to be 49.9 ± 5.5, 1.3 ± 0.2, 1.4 ± 0.3, 1.3 ± 0.3 and 715.8 ± 45.1 nM, respectively

Radiochemistry

^{111}In(DOTA-3P-RGD$_2$), ^{111}In(DTPA-3P-RGD$_2$) and ^{111}In(DTPA-Bn-3P-RGD$_2$) were prepared by reacting ^{111}InCl$_3$ with respective RGD conjugate in NH$_4$OAc buffer (100 mM, pH 5.5). For ^{111}In(DOTA-3P-RGD$_2$), radiolabeling could be completed by heating the reaction mixture at 100°C for 15–20 min. For ^{111}In(DTPA-3P-RGD$_2$) and ^{111}In(DTPA-Bn-3P-RGD$_2$), chelation was almost instantaneous at room temperature. The RCP was >95% without purification. The specific activity was ~100 mCi/μmol for ^{111}In(DOTA-3P-RGD$_2$) while it was ~400 mCi/μmol for ^{111}In(DTPA-3P-RGD$_2$) and ^{111}In(DTPA-Bn-3P-RGD$_2$). All new ^{111}In radiotracers were analyzed using the same method (Method 3). As expected, they all remained stable for >24 h both in saline and in 6 mM EDTA solution. Their HPLC retention times and log *P* values were listed in Table 1.

Biodistribution characteristics

The athymic nude mice bearing U87MG glioma xenografts were used to evaluate biodistribution properties of ^{111}In(DOTA-3P-RGD$_2$), ^{111}In(DTPA-3P-RGD$_2$) and ^{111}In(DTPA-Bn-3P-RGD$_2$) to assess the impact of BFC on tumor uptake and pharmacokinetics of the ^{111}In radiotracers. The biodistribution data are summarized in Tables 2, 3, and 4. In general, the tumor uptake of ^{111}In(DOTA-3P-RGD$_2$) was

Table 1 Radiochemical purity (RCP), HPLC retention time and log *P* values for ^{111}In-labeled cyclic RGD peptide dimers

Compound	RCP (%)	Retention time (min)	Log *P* value
^{111}In(DOTA-3P-RGD$_2$)	>97	19.61	−4.20 ± 0.21
^{111}In(DTPA-3P-RGD$_2$)	>95	19.30	−3.91 ± 0.07
^{111}In(DTPA-Bn-3P-RGD$_2$)	>92	21.10	−3.50 ± 0.04
^{111}In(DOTA-3P-RGK$_2$)	>97	19.94	−4.03 ± 0.05

high (10.89 ± 2.55, 9.20 ± 5.35, 7.65 ± 3.17, 6.50 ± 1.71 and 2.18 ± 0.63%ID/g at 0.5, 1, 4, 24 and 72 h p.i., respectively) with a rapid blood clearance. As a result, its tumor/blood ratios were very high (19.76 ± 5.42, 39.63 ± 20.61, 99.93 ± 49.2, 110.82 ± 49.67 and 101.7 ± 58.4 at 0.5, 1, 4, 24 and 72 h p.i., respectively. The liver uptake of ^{111}In(DOTA-3P-RGD$_2$) was very low (2.21 ± 0.53, 1.55 ± 0.37, 1.66 ± 0.21, 0.62 ± 0.11 and 0.25 ± 0.05%ID/g at 0.5, 1, 4, 24 and 72 h p.i., respectively) with high tumor/liver ratios (5.90 ± 2.61, 6.19 ± 1.34, 5.09 ± 2.41, 9.59 ± 3.31 and 8.95 ± 3.73 at 0.5, 1, 4, 24 and 72 h p.i., respectively). The kidney uptake of ^{111}In(DOTA-3P-RGD$_2$) was also low with tumor/kidney ratio increasing steadily over the 72-h period (Table 2). Figure 3 compares the glioma uptake (%ID/g) and T/B ratios of ^{111}In(DOTA-3P-RGD$_2$), ^{111}In(DTPA-3P-RGD$_2$) and ^{111}In(DTPA-Bn-3P-RGD$_2$). The initial tumor uptake of ^{111}In(DTPA-3P-RGD$_2$) (9.82 ± 1.52 and 5.25 ± 2.29%ID/g at 0.5 and 4 h p.i., respectively) and ^{111}In(DTPA-Bn-3P-RGD$_2$) (9.79 ± 3.44 and 6.13 ± 0.82%ID/g at 0.5 and 4 h p.i., respectively) was very close to that of ^{111}In(DOTA-3P-RGD$_2$). However, their tumor uptake between 24 and 72 h p.i. was significantly ($P < 0.01$) lower than that of ^{111}In(DOTA-3P-RGD$_2$) (Fig. 3). The tumor/blood, tumor/liver and tumor/lung ratios of ^{111}In(DTPA-3P-RGD$_2$) and ^{111}In(DTPA-Bn-3P-RGD$_2$) were significantly generally lower than those of ^{111}In(DOTA-3P-RGD$_2$) over the 72-h study period. This is particularly true between 24 and 72 h p.i. due to a faster tumor washout of ^{111}In(DTPA-3P-RGD$_2$) and ^{111}In(DTPA-Bn-3P-RGD$_2$). It is quite clear that the BFC has a significant impact on both tumor uptake and T/B ratios.

Integrin $\alpha_v\beta_3$ specificity

This experiment was designed to demonstrate the integrin $\alpha_v\beta_3$ specificity using RGD$_2$ (14 mg/kg or ~350 μg/mouse) as the blocking agent and ^{111}In(DOTA-3P-RGD$_2$) as the radiotracer. Figure 4a compares the organ uptake of ^{111}In(DOTA-3P-RGD$_2$) in the absence/presence of RGD$_2$ at 60 min p.i. Co-injection of excess RGD$_2$ almost completely blocked the tumor uptake of ^{111}In(DOTA-3P-RGD$_2$) (0.29 ± 0.04%ID/g with RGD$_2$ vs. 9.20 ± 5.35%ID/g without RGD$_2$). The normal organ uptake of ^{111}In(DOTA-3P-RGD$_2$) was also significantly blocked by excess RGD$_2$. For example, the uptake of ^{111}In(DOTA-3P-RGD$_2$) in the eyes, heart, intestine, kidneys, liver, lungs, muscle and spleen was 0.74 ± 0.22, 0.57 ± 0.16, 4.07 ± 1.39, 3.83 ± 0.85, 1.55 ± 0.37, 1.72 ± 0.50, 0.77 ± 0.31 and 1.50 ± 0.43%ID/g, respectively, without RGD$_2$) while its uptake in the eyes, heart, intestine, kidneys, liver, lungs, muscle and spleen was only 0.10 ± 0.03, 0.10 ± 0.00, 0.25 ± 0.10, 1.79 ± 0.27, 0.15 ± 0.02, 0.35 ± 0.05,

Table 2 Selected biodistribution data of ^{111}In(DOTA-3P-RGD$_2$) in the athymic nude mice ($n = 5$) bearing U87MG human glioma xenografts

%ID/g	0.5 h	1 h	4 h	24 h	72 h
Blood	0.62 ± 0.13	0.23 ± 0.06	0.06 ± 0.03	0.05 ± 0.03	0.03 ± 0.01
Bone	1.50 ± 0.20	1.23 ± 0.23	0.96 ± 0.02	0.53 ± 0.10	0.39 ± 0.12
Brain	0.16 ± 0.06	0.09 ± 0.02	0.06 ± 0.01	0.05 ± 0.01	0.04 ± 0.01
Eyes	0.85 ± 0.12	0.74 ± 0.22	0.58 ± 0.18	0.33 ± 0.05	0.19 ± 0.03
Heart	0.83 ± 0.13	0.57 ± 0.16	0.44 ± 0.08	0.28 ± 0.06	0.14 ± 0.02
Intestine	5.55 ± 1.05	4.07 ± 1.39	3.82 ± 1.71	3.12 ± 1.40	1.20 ± 0.39
Kidney	5.80 ± 0.95	3.83 ± 0.85	2.87 ± 0.20	2.01 ± 0.24	0.98 ± 0.16
Liver	2.21 ± 0.53	1.55 ± 0.37	1.66 ± 0.21	0.62 ± 0.11	0.25 ± 0.05
Lungs	2.67 ± 0.32	1.72 ± 0.50	1.17 ± 0.23	0.66 ± 0.14	0.22 ± 0.02
Muscle	0.90 ± 0.17	0.77 ± 0.31	0.55 ± 0.17	0.41 ± 0.09	0.26 ± 0.11
Spleen	1.57 ± 0.28	1.50 ± 0.43	1.36 ± 0.47	1.01 ± 0.22	0.41 ± 0.07
U87MG	10.89 ± 2.55	9.20 ± 5.35	7.65 ± 3.17	6.50 ± 1.71	2.18 ± 0.63
Tumor/blood	19.76 ± 5.42	39.63 ± 20.61	99.93 ± 49.2	110.8 ± 46.5	101.7 ± 58.4
Tumor/kidney	2.16 ± 0.72	2.52 ± 1.34	2.98 ± 1.32	2.99 ± 1.07	2.22 ± 0.65
Tumor/liver	5.90 ± 2.61	6.19 ± 1.34	5.09 ± 2.41	9.59 ± 3.31	8.95 ± 3.73
Tumor/lungs	4.60 ± 1.58	5.31 ± 2.02	7.15 ± 2.44	8.36 ± 2.58	10.48 ± 2.69
Tumor/muscle	13.34 ± 4.37	11.62 ± 3.98	15.13 ± 3.22	15.19 ± 5.01	8.21 ± 3.18

Table 3 Biodistribution data of ^{111}In(DTPA-3P-RGD$_2$) in the athymic nude mice ($n = 5$) bearing U87MG human glioma xenografts

%ID/g	0.5 h	1 h	4 h	24 h	72 h
Blood	1.11 ± 0.37	0.30 ± 0.10	0.07 ± 0.03	0.05 ± 0.02	0.02 ± 0.00
Bone	1.71 ± 0.25	1.19 ± 0.16	0.83 ± 0.12	0.57 ± 0.09	0.23 ± 0.14
Brain	0.14 ± 0.02	0.09 ± 0.01	0.07 ± 0.01	0.05 ± 0.01	0.03 ± 0.01
Eyes	1.16 ± 0.24	0.70 ± 0.35	0.58 ± 0.09	0.28 ± 0.17	0.16 ± 0.06
Heart	1.19 ± 0.38	0.65 ± 0.24	0.54 ± 0.16	0.27 ± 0.05	0.12 ± 0.03
Intestine	9.45 ± 2.69	7.83 ± 1.64	6.89 ± 2.72	5.11 ± 1.45	2.03 ± 0.87
Kidney	8.76 ± 2.40	5.33 ± 0.46	3.37 ± 0.70	2.26 ± 0.47	0.92 ± 0.20
Liver	3.18 ± 0.75	2.20 ± 0.13	1.46 ± 0.27	0.84 ± 0.08	0.31 ± 0.08
Lungs	3.85 ± 0.71	2.11 ± 0.22	1.35 ± 0.20	0.82 ± 0.05	0.26 ± 0.05
Muscle	1.09 ± 0.25	0.65 ± 0.07	0.60 ± 0.24	0.30 ± 0.07	0.12 ± 0.04
Spleen	2.51 ± 0.75	1.86 ± 0.28	1.54 ± 0.28	1.09 ± 0.06	0.33 ± 0.08
U87MG	9.82 ± 1.52	8.60 ± 2.17	5.25 ± 2.29	4.08 ± 0.78	1.36 ± 0.28
Tumor/blood	9.93 ± 4.49	32.94 ± 14.75	72.76 ± 21.78	95.31 ± 31.50	86.11 ± 35.19
Tumor/bone	5.89 ± 1.37	7.17 ± 1.16	6.31 ± 2.39	7.26 ± 1.67	7.94 ± 5.12
Tumor/kidney	1.17 ± 0.30	1.60 ± 0.30	1.63 ± 0.76	1.82 ± 0.47	1.51 ± 0.31
Tumor/liver	3.20 ± 0.74	3.95 ± 1.00	3.60 ± 1.26	4.89 ± 1.02	4.56 ± 1.07
Tumor/lungs	2.62 ± 0.62	4.02 ± 0.74	4.01 ± 1.93	4.95 ± 0.93	5.31 ± 1.00
Tumor/muscle	9.42 ± 2.62	13.34 ± 2.81	10.01 ± 5.03	14.31 ± 3.98	12.63 ± 4.01

Table 4 Selected biodistribution data of ^{111}In(DTPA-Bn-3P-RGD$_2$) in the athymic nude mice ($n = 5$) bearing U87MG human glioma xenografts

%ID/g	0.5 h	1 h	4 h	24 h	72 h
Blood	0.52 ± 0.02	0.24 ± 0.04	0.06 ± 0.02	0.03 ± 0.01	0.02 ± 0.01
Bone	0.82 ± 0.22	0.65 ± 0.14	0.52 ± 0.13	0.49 ± 0.14	0.51 ± 0.11
Brain	0.13 ± 0.03	0.12 ± 0.01	0.06 ± 0.01	0.03 ± 0.00	0.02 ± 0.00
Eyes	0.89 ± 0.20	0.97 ± 0.08	0.52 ± 0.03	0.18 ± 0.03	0.10 ± 0.01
Heart	0.88 ± 0.05	0.69 ± 0.06	0.41 ± 0.02	0.13 ± 0.02	0.06 ± 0.00
Intestine	5.09 ± 2.23	3.70 ± 0.40	2.64 ± 0.47	0.76 ± 0.06	0.37 ± 0.06
Kidney	6.24 ± 0.33	4.83 ± 0.46	4.01 ± 0.60	1.42 ± 0.33	0.50 ± 0.01
Liver	2.40 ± 0.12	2.02 ± 0.02	1.47 ± 0.15	0.37 ± 0.06	0.16 ± 0.03
Lungs	2.63 ± 0.12	1.97 ± 0.11	1.30 ± 0.13	0.42 ± 0.06	0.11 ± 0.01
Muscle	0.89 ± 0.17	1.11 ± 0.08	0.89 ± 0.60	0.14 ± 0.01	0.17 ± 0.05
Spleen	1.45 ± 0.09	1.55 ± 0.12	1.72 ± 0.15	0.60 ± 0.14	0.28 ± 0.03
U87MG	9.79 ± 3.44	5.62 ± 0.88	6.13 ± 0.82	2.03 ± 0.24	0.45 ± 0.05
Tumor/blood	18.89 ± 7.03	24.06 ± 7.04	108.06 ± 14.30	98.21 ± 7.13	36.18 ± 12.11
Tumor/kidney	1.57 ± 0.54	1.18 ± 0.27	1.53 ± 0.11	1.47 ± 0.30	0.96 ± 0.10
Tumor/liver	4.05 ± 1.31	2.78 ± 0.44	4.19 ± 0.39	5.54 ± 0.83	2.71 ± 0.16
Tumor/lungs	3.68 ± 1.17	2.85 ± 0.40	4.71 ± 0.32	4.86 ± 0.47	4.10 ± 0.17
Tumor/muscle	11.70 ± 6.04	5.10 ± 0.96	8.92 ± 4.25	14.64 ± 1.05	3.81 ± 1.42

0.14 ± 0.06 and 0.11 ± 0.00%ID/g, respectively, with RGD$_2$.

RGD specificity

Figure 4b compares the 60-min uptake of ^{111}In(DOTA-3P-RGD$_2$) and ^{111}In(DOTA-3P-RGK$_2$) in the tumor and normal organs. As expected, ^{111}In(DOTA-3P-RGK$_2$) had much lower tumor uptake (0.30 ± 0.09%ID/g) than ^{111}In(DOTA-3P-RGD$_2$) (9.20 ± 5.35%ID/g). ^{111}In(DOTA-3P-RGK$_2$) also had significantly ($P < 0.01$) lower uptake in normal organs than ^{111}In(DOTA-3P-RGD$_2$). For example, the uptake of ^{111}In(DOTA-3P-RGK$_2$) in intestine, kidneys, liver, lungs and spleen was 0.74 ± 0.28,

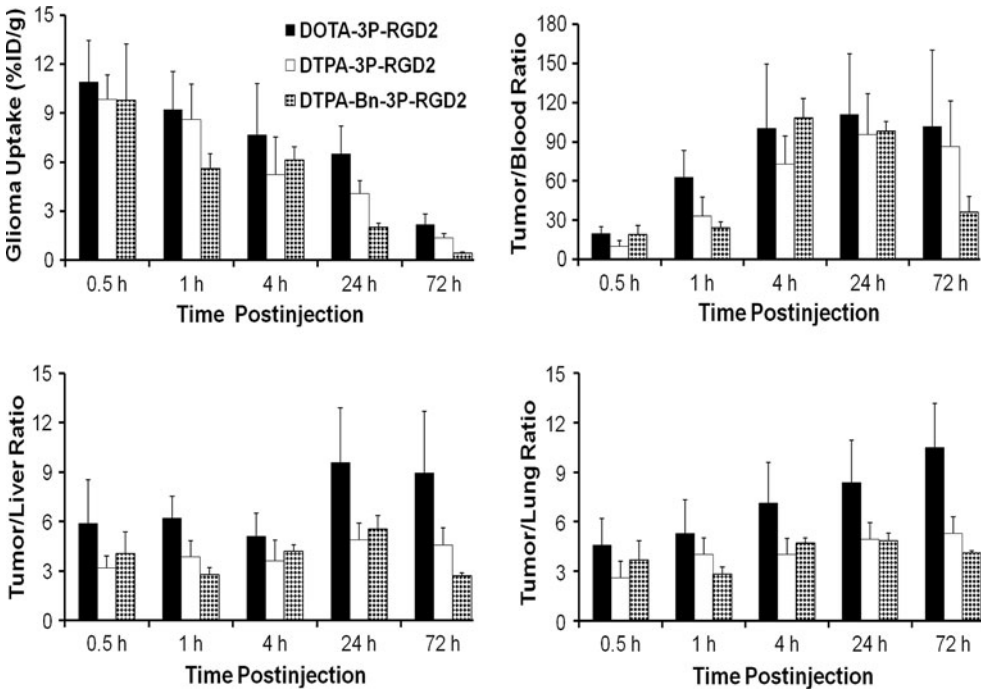

Fig. 3 Comparison of glioma uptake (%ID/g) and T/B ratios between ^{111}In(DOTA-3P-RGD$_2$), ^{111}In(DTPA-3P-RGD$_2$) and ^{111}In(DTPA-Bn-3P-RGD$_2$) in athymic nude mice ($n = 5$) bearing U87MG human glioma xenografts

3.19 ± 0.56, 0.19 ± 0.01, 0.41 ± 0.17 and 0.19 ± 0.17%ID/g, respectively, while the uptake of ^{111}In(DOTA-3P-RGD$_2$) was 4.07 ± 1.39, 3.83 ± 0.85, 1.55 ± 0.37, 1.72 ± 0.50 and 1.50 ± 0.43%ID/g in the same organs, respectively. The blood radioactivity of ^{111}In(DOTA-3P-RGK$_2$) (0.62 ± 0.55%ID/g) was higher ($P < 0.01$) than that of ^{111}In(DOTA-3P-RGD$_2$) (0.23 ± 0.06%ID/g).

Planar imaging study

Figure 5 illustrates planar images of the glioma-bearing mouse administered with ~100 μCi of ^{111}In(DOTA-3P-RGD$_2$) and ^{111}In(DTPA-3P-RGD$_2$) at 24 h p.i. The tumors larger than 0.1 g (~100 mm^3) could be clearly visualized with excellent T/B contrast as early as 1 h p.i. Both ^{111}In(DOTA-3P-RGD$_2$) and ^{111}In(DTPA-3P-RGD$_2$) were able to retain in the tumor for a very long time (>72 h), which is consistent with the biodistribution data (Tables 2, 3). In addition, the radioactivity distribution pattern in the same tumor was quite heterogeneous in the mouse administered with of ^{111}In(DOTA-3P-RGD$_2$). Because of the radioactivity accumulation in the abdominal region, it was difficult to accurately determine the tumor/kidney and tumor/liver ratios on the basis of planar imaging.

Metabolism

Normal athymic nude mice were used to examine the metabolic stability of ^{111}In(DOTA-3P-RGD$_2$) and ^{111}In(DTPA-Bn-3P-RGD$_2$) during excretion. We found that the percentage radioactivity recovery was >95% (by γ-counting) for the collected urine and feces samples. Attempts to extract radioactivity from the liver and kidney tissues were not successful due to limited radioactivity accumulation in both organs. Figure 6 shows radio-HPLC chromatograms of ^{111}In(DOTA-3P-RGD$_2$) and ^{111}In(DTPA-Bn-3P-RGD$_2$) in saline before injection, in urine at 30 and 120 min p.i., and in feces at 120 min p.i. ^{111}In(DOTA-3P-RGD$_2$) had very little metabolite detected in either urine or feces over the 2-h period. However, only ~25% of ^{111}In(DTPA-Bn-3P-RGD$_2$) remained intact in the feces sample, whereas it was nearly intact in the urine sample during 2-h study period. ^{111}In(DTPA-3P-RGD$_2$) also exhibited similar metabolic properties as ^{111}In(DTPA-Bn-3P-RGD$_2$).

Discussion

In this study, we found that the integrin $\alpha_v\beta_3$-binding affinity follows the order of DOTA-3P-RGD$_2$ ~ DTPA-3P-RGD$_2$ ~ DTPA-Bn-3P-RGD$_2$ > c(RGDfK) ≫ DOTA-3P-RGK$_2$. The higher integrin $\alpha_v\beta_3$-binding affinity of DOTA-3P-RGD$_2$, DTPA-3P-RGD$_2$ and DTPA-3P-RGD$_2$ as compared to that of c(RGDfK) is likely caused by their bivalency in binding to the integrin $\alpha_v\beta_3$. The fact that DOTA-3P-RGD$_2$, DTPA-3P-RGD$_2$ and DTPA-Bn-3P-RGD$_2$ share almost identical integrin $\alpha_v\beta_3$-binding affinity (Fig. 2) suggests that the BFC (DOTA, DTPA and DTPA-Bn) has little impact on their integrin $\alpha_v\beta_3$-targeting capability.

^{111}In(DOTA-3P-RGD$_2$), ^{111}In(DTPA-3P-RGD$_2$) and ^{111}In(DTPA-Bn-3P-RGD$_2$) share the same biomolecule 3P-RGD$_2$. The advantage of using DTPA as BFC is its high

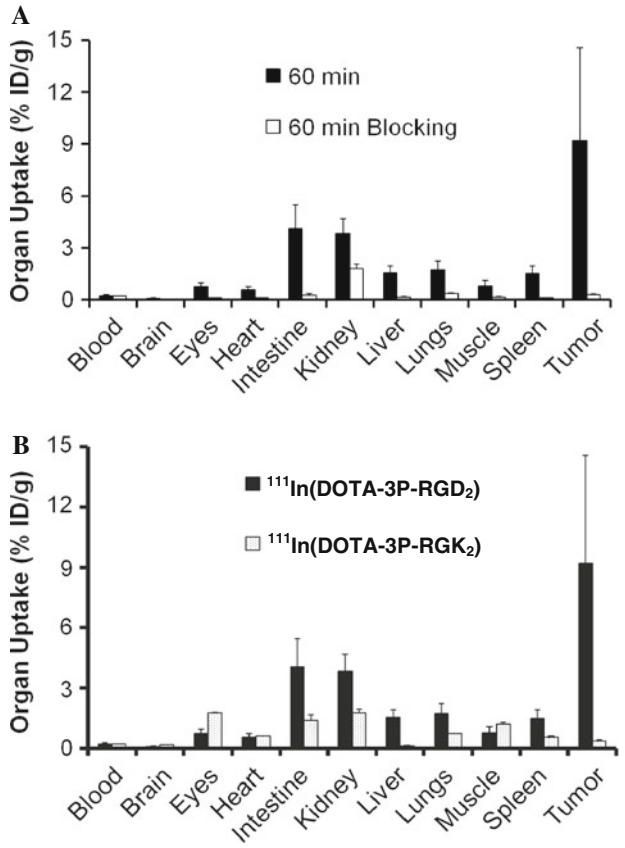

Fig. 4 *Top* comparison of the 60-min biodistribution data of ^{111}In(DOTA-3P-RGD$_2$) in athymic nude mice ($n = 5$) bearing U87MG glioma xenografts in the absence/presence of excess E[c(RGDfK)]$_2$ to demonstrate its integrin $\alpha_v\beta_3$-specificity; *bottom* comparison of the 60-min biodistribution data of ^{111}In(DOTA-3P-RGD$_2$) and ^{111}In(DOTA-3P-RGK$_2$) in athymic nude mice ($n = 5$) bearing U87MG glioma xenografts to demonstrate the RGD-specificity

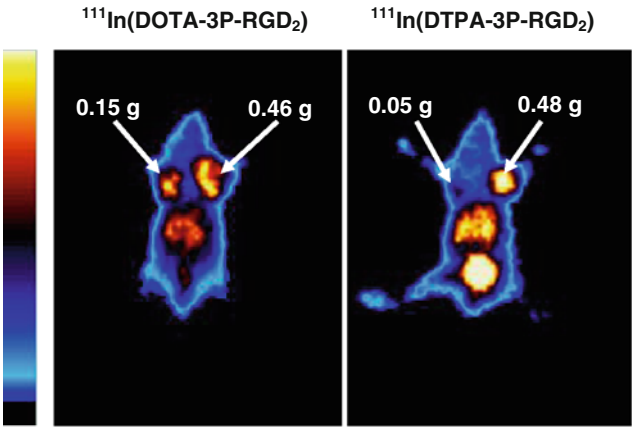

Fig. 5 Planar images of the athymic nude mice (bearing U87MG human glioma xenografts) administered with ~100 μCi of ^{111}In(DOTA-3P-RGD$_2$) and ^{111}In(DTPA-3P-RGD$_2$) at 24 h p.i

radiolabeling efficiency (fast and high yield radiolabeling), which is very important for receptor-specific radiotracers. For example, ^{111}In(DTPA-3P-RGD$_2$) and ^{111}In(DTPA-Bn-3P-RGD$_2$) could be readily prepared at room temperature. Their specific activity is >4× higher than that of ^{111}In(DOTA-3P-RGD$_2$). Thus, ^{111}In(DTPA-3P-RGD$_2$) and ^{111}In(DTPA-Bn-3P-RGD$_2$) have a significant advantage over ^{111}In(DOTA-3P-RGD$_2$), if imaging can be completed within 4 h p.i. and high-specific activity is absolutely required. In addition, all three radiotracers share similar tumor uptake over the first 4 h (Fig. 3). Based on these results, it is concluded that ^{111}In(DOTA-3P-RGD$_2$), ^{111}In(DTPA-3P-RGD$_2$) and ^{111}In(DTPA-Bn-3P-RGD$_2$) are all useful for imaging tumor integrin $\alpha_v\beta_3$. This conclusion is completely supported by the results from planar imaging studies (Fig. 5).

However, ^{111}In(DOTA-3P-RGD$_2$) has a slower tumor washout kinetics (Fig. 3) than ^{111}In(DTPA-3P-RGD$_2$) and ^{111}In(DTPA-Bn-3P-RGD$_2$). As a result, ^{111}In(DOTA-3P-RGD$_2$) has better ($P < 0.01$) tumor/liver and tumor/kidney ratios than ^{111}In(DTPA-3P-RGD$_2$) and ^{111}In(DTPA-Bn-3P-RGD$_2$). In addition, ^{111}In(DOTA-3P-RGD$_2$) has better metabolic stability (Fig. 6) than ^{111}In(DTPA-Bn-3P-RGD$_2$) during hepatobiliary excretion. This is most likely caused by the kinetic inertness of the ^{111}In-DOTA chelate. The kinetic instability of ^{111}In-labeled DTPA-biomolecule conjugates has been well-documented (Smith-Jones et al. 2000; Aloj et al. 2004; Liu 2004, 2008), and release of ^{111}In often results in higher radioactivity accumulation in the liver and lungs because of its high affinity for transferrin (Ando et al. 1989). This conclusion is also consistent with the slightly higher uptake of ^{111}In(DTPA-3P-RGD$_2$) in the liver and lungs (Table 3) as compared to that of ^{111}In(DOTA-3P-RGD$_2$) (Table 2).

The integrin $\alpha_v\beta_3$-specificity of ^{111}In(DOTA-3P-RGD$_2$) was demonstrated by the blocking experiment (Fig. 4a), in which RGD$_2$ was used as the blocking agent. The uptake blockage in the eyes, heart, intestine, lungs, liver and spleen suggests that the radioactivity accumulation of ^{111}In(DOTA-3P-RGD$_2$) in these organs is also integrin $\alpha_v\beta_3$-mediated. This conclusion is supported by immunohistopathological studies (Wu et al. 2007a, b), which showed a strong positive staining of endothelial cells of small glomeruli vessels in the kidneys and weak staining in branches of the hepatic portal vein. The RGD-specificity for the tumor localization of ^{111}In(DOTA-3P-RGD$_2$) has been demonstrated by the low integrin $\alpha_v\beta_3$-binding affinity of DOTA-3P-RGK$_2$ (Fig. 2) and low tumor uptake of ^{111}In(DOTA-3P-RGK$_2$) (Fig. 4b). In addition, ^{111}In(DOTA-3P-RGK$_2$) also has low uptake in the intestine, kidneys, liver, lungs and spleen (Fig. 4b), further suggesting that the high uptake of ^{111}In(DOTA-3P-RGD$_2$) in these organs is also RGD-specific. The higher blood radioactivity of ^{111}In(DOTA-3P-RGK$_2$) as compared to that of ^{111}In(DOTA-3P-RGD$_2$) is most likely caused by its lower uptake in normal organs.

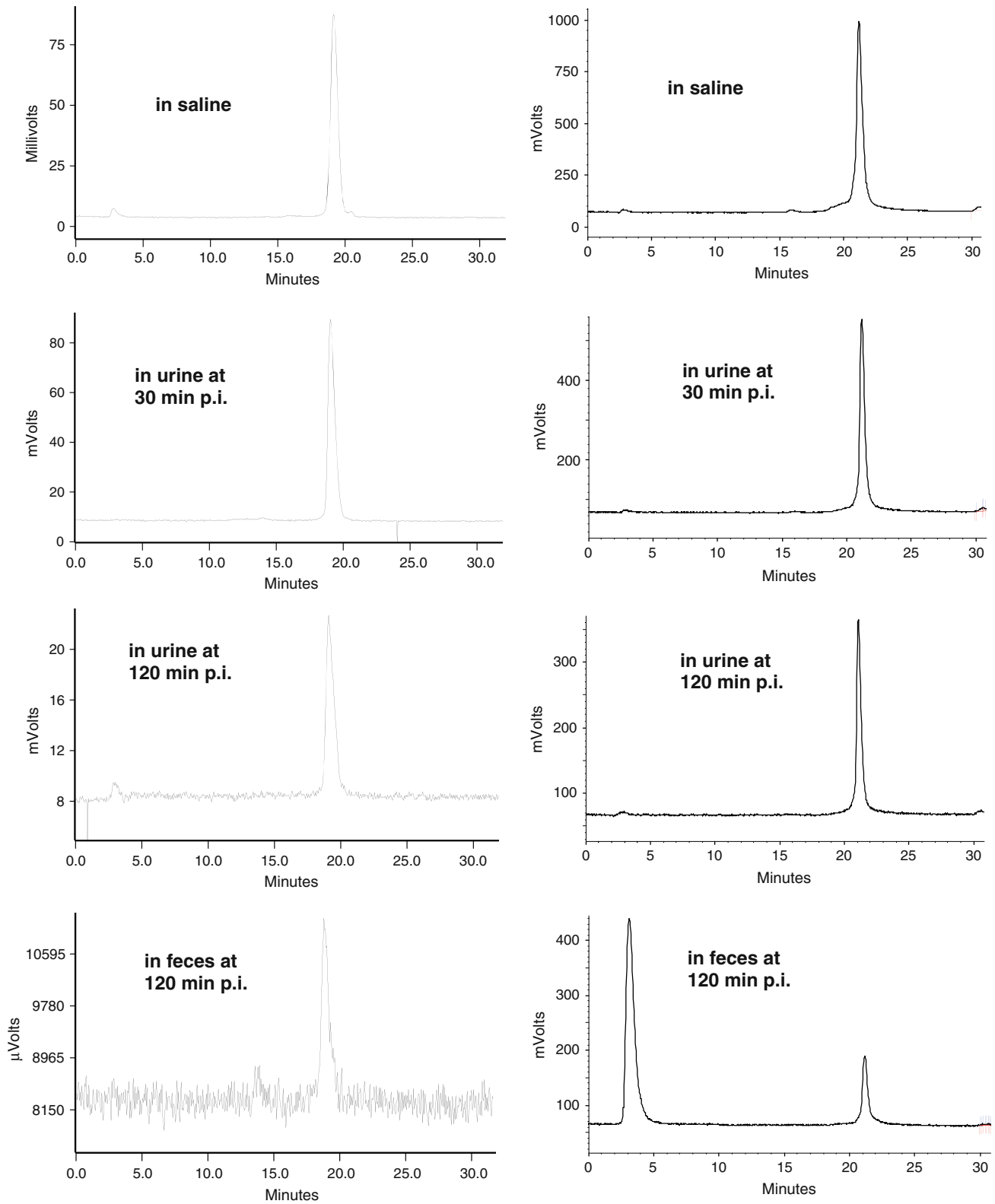

Fig. 6 Typical radio-HPLC chromatograms of ^{111}In(DOTA-3P-RGD$_2$) (*left*) and ^{111}In(DTPA-Bn-3P-RGD$_2$) (*right*) in saline before injection, in urine at 30 and 120 min p.i., and in feces at 120 min p.i. Each mouse was administered with ~100 µCi radiotracer. Two normal mice were used for each radiotracer

Conclusion

This report presents the biological evaluation of ^{111}In(DOTA-3P-RGD$_2$), ^{111}In(DTPA-3P-RGD$_2$) and ^{111}In (DTPA-Bn-3P-RGD$_2$) as potential radiotracers for imaging integrin $\alpha_v\beta_3$ expression. The key findings of this study are: (1) BFC has little impact on the integrin $\alpha_v\beta_3$-binding affinity of a cyclic RGD peptide dimer (3P-RGD$_2$); (2) ^{111}In(DTPA-3P-RGD$_2$) can be readily prepared at room temperature with specific activity >4× of that for ^{111}In(DOTA-3P-RGD$_2$); (3) all the three radiotracers have very high tumor uptake and excellent T/B ratios up to 4 h p.i.; (4) ^{111}In(DTPA-3P-RGD$_2$) can be used as an integrin $\alpha_v\beta_3$-targeted radiotracer if high-specific activity is required. However, DOTA remains to be the candidate of choice for the development of therapeutic lanthanide radiotracers.

Acknowledgments This work is supported, in part, by Purdue University and research grants: R01 CA115883-A2 from National Cancer Institute (NCI), R21 HL08396-01 from National Heart, Lung, and Blood Institute (NHLBI), and DE-FG02-08ER64684 from the Department of Energy.

References

Aloj L, Cacraco C, Panico M, Zannetti A, Del Vecchio S, Tesauro D, De Luca S, Arra C, Pedone C, Morelli G, Salvatore M (2004) In vitro and in vivo evaluation of ^{111}In-DTPAGlu-G-CCK8 for cholecystokinin-B-receptor imaging. J Nucl Med 45:485–494

Ando A, Ando I, Hiraki T, Hishada K (1989) Relation between the location of the elements in the periodic table and various organ uptake rates. Nucl Med Biol 16:57–80

Bakker WH, Albert R, Bruns C, Breeman WA, Hofland LJ, Marbach P, Pless J, Pralet D, Stolz B, Koper JW, Lamberts SWJ, Visser TJ, Krenning EP (1991) [^{111}In-DTPA-D-Phe^1]-octreotide, a potential radiopharmaceutical for imaging of somatostatin receptor-positive tumors: synthesis, radiolabeling and in vitro validation. Life Sci 49:1583–1591

Beer AJ, Haubner R, Goebel M, Luderschmidt S, Spilker ME, Wester HJ, Weber WA, Schwaiger M (2005) Biodistribution and pharmacokinetics of the $\alpha_v\beta_3$-selective tracer ^{18}F-Galacto-RGD in cancer patients. J Nucl Med 46:1333–1341

Bodei L, Cremonesi M, Grana C, Rocca P, Bartolomei M, Chinol M, Paganelli G (2004) Receptor radionuclide therapy with ^{90}Y-[DOTA]^0-Tyr^3-octreotide (^{90}Y-DOTATOC) in neuroendocrine tumors. Eur J Nucl Med Mol Imaging 31:1038–1046

Chen X (2006) Multimodality imaging of tumor integrin $\alpha_v\beta_3$ expression. Mini Rev Med Chem 6:227–234

Chen X, Liu S, Hou Y, Tohme M, Park R, Bading JR, Conti PS (2004a) MicroPET imaging of breast cancer α_v-integrin expression with ^{64}Cu-labeled dimeric RGD peptides. Mol Imaging Biol 6:350–359

Chen X, Park R, Hou Y, Tohme M, Shahinian AH, Banding JR, Conti PS (2004b) MicroPET and autoradiographic imaging of CRP receptor expression with ^{64}Cu-DOTA-[Lys^3]bombesin in human prostate adenocarcinoma xenografts. J Nucl Med 45:1390–1397

Chen X, Park R, Tohme M, Shahinian AH, Bading JR, Conti PS (2004c) MicroPET and autoradiographic imaging of breast cancer α_v-integrin expression using ^{18}F- and ^{64}Cu-labeled RGD peptide. Bioconj Chem 15:41–49

Chen X, Tohme M, Park R, Hou Y, Bading JR, Conti PS (2004d) MicroPET imaging of breast cancer α_v-integrin expression with ^{18}F-labeled dimeric RGD peptide. Mol Imaging 3:96–104

de Visser M, Bernard HF, Erion JL, Schmidt MA, Srinivasan A, Waser B, Reubi JC, Krenning EP, de Jong M (2007) Novel ^{111}In-labelled bombesin analogues for molecular imaging of prostate tumors. Eur J Nucl Med Mol Imaging 34:1228–1238

Decristoforo C, Faintuch-Linkowski B, Rey A, von Guggenberg E, Rupprich M, Hernandez-Gonzales I, Rodrigo T, Haubner R (2006) [^{99m}Tc]HYNIC-RGD for imaging integrin $\alpha_v\beta_3$ expression. Nucl Med Biol 33:945–952

Dijkgraaf I, Kruijtzer JAW, Liu S, Soede A, Oyen WJG, Corstens FHM, Liskamp RMJ, Boerman OC (2007a) Improved targeting of the $\alpha_v\beta_3$ integrin by multimerization of RGD peptides. Eur J Nucl Med Mol Imaging 34:267–273

Dijkgraaf I, Liu S, Kruijtzer JAW, Soede AC, Oyen WJG, Liskamp RMJ, Corstens FHM, Boerman OC (2007b) Effect of linker variation on the in vitro and in vivo characteristics of an ^{111}In-labeled RGD peptide. Nucl Med Biol 34:29–35

Haubner R, Wester HJ, Reuning U, Senekowisch-Schmidtke R, Diefenbach B, Kessler H, Stöcklin G, Schwaiger M (1999) Radiolabeled $\alpha_v\beta_3$ integrin antagonists: a new class of tracers for tumor imaging. J Nucl Med 40:1061–1071

Heppeler A, Froidevaux S, Mäcke HR, Jermann E, Béhé M, Powell P, Hennig M (1999) Radiometal-labelled macrocyclic chelator-derivatised somatostatin analogue with superb tumour targeting properties and potential for receptor-mediated internal radiotherapy. Chem Eur J 5:1974–1981

Janssen ML, Oyen WJG, Dijkgraaf I, Massuger LF, Frielink C, Edwards DS, Rajopadhye M, Boonstra H, Corstens FH, Boerman OC (2002) Tumor targeting with radiolabeled $\alpha_v\beta_3$ integrin binding peptides in a nude mouse model. Cancer Res 62:6146–6151

Jia B, Shi J, Yang Z, Xu B, Liu Z, Zhao H, Liu S, Wang F (2006) ^{99m}Tc-labeled cyclic RGDfK dimer: initial evaluation for SPECT imaging of glioma integrin $\alpha_v\beta_3$ expression. Bioconj Chem 17:1069–1076

Jia B, Liu Z, Shi J, Yu ZL, Yang Z, Zhao HY, He ZJ, Liu S, Wang F (2008) Linker effects on biological properties of ^{111}In-labeled DTPA conjugates of a cyclic RGDfK dimer. Bioconj Chem 19:201–210

Kenny LM, Coombes RC, Oulie I, Contractor KB, Miller M, Spinks TJ, McParland B, Cohen PS, Hui A, Palmieri C, Osman S, Glaser M, Turton D, Al-Nahhas A, Aboagye EO (2008) Phase I trial of the positron-emitting Arg-Gly-Asp (RGD) peptide radioligand ^{18}F-AH111585 in breast cancer patients. J Nucl Med 49:879–886

Koukouraki S, Strauss LG, Georgoulias V, Schuhmacher J, Haberkorn U, Karkavitsas N, Dimitrakopoulou-Strauss A (2006) Evaluation of the pharmacokinetics of ^{68}Ga-DOTATOC in patients with metastatic neuroendocrine tumours scheduled for ^{90}Y-DOTATOC therapy. Eur J Nucl Med Mol Imaging 33:460–466

Kowalski J, Henze M, Schuhmacher J, Macke HR, Hofmann M, Haberkorn U (2003) Evaluation of positron emission tomography imaging using ^{68}Ga-DOTA-D-Phe^1-Tyr^3-octreotide in comparison to ^{111}In-DTPAOC SPECT. First results in patients with neuroendocrine tumors. Mol Imaging Biol 5:42–48

Kwekkeboom DJ, de Herder WW, Kam BL, van Eijck CK, van Essen M, Kooij PP, Feelders RA, van Aken MO, Krenning EP (2008) Treatment with the radiolabeled somatostatin analog [^{177}Lu-DOTA0, Tyr3]octreotate: toxicity, efficacy and survival. J Clin Oncol 26:2114–2130

Liu S (2004) The role of coordination chemistry in development of target-specific radiopharmaceuticals. Chem Soc Rev 33:445–461

Liu S (2006) Radiolabeled multimeric cyclic RGD peptides as integrin $\alpha_v\beta_3$-targeted radiotracers for tumor imaging. Mol Pharm 3:472–487

Liu S (2008) Bifunctional coupling agents for radiolabeling of biomolecules and target-specific delivery of metallic radionuclides. Adv Drug Deliv Rev 60:1347–1370

Liu S, Edwards DS (2001a) Bifunctional chelators for therapeutic lanthanide radiopharmaceuticals. Bioconj Chem 12:7–34

Liu S, Edwards DS (2001b) Synthesis and characterization of two ^{111}In-labeled DTPA-peptide conjugates. Bioconj Chem 12:630–634

Liu S, Cheung E, Rajopadyhe M, Ziegler MC, Edwards DS (2001a) ^{90}Y- and ^{177}Lu-labeling of a DOTA conjugated vitronectin receptor antagonist for tumor therapy. Bioconj Chem 12:559–568

Liu S, Edwards DS, Ziegler MC, Harris AR, Hemingway SJ, Barrett JA (2001b) ^{99m}Tc-labeling of a hydrazinonictotinamide-conjugated vitronectin receptor antagonist. Bioconj Chem 12:624–629

Liu S, Robinson SP, Edwards DS (2003) Integrin $\alpha_v\beta_3$ directed radiopharmaceuticals for tumor imaging. Drugs Future 28:551–564

Liu S, Hsieh WY, Jiang Y, Kim YS, Sreerama SG, Chen X, Jia B, Wang F (2007) Evaluation of a ^{99m}Tc-labeled cyclic RGD tetramer for non-invasive imaging integrin $\alpha_v\beta_3$-positive breast cancer. Bioconj Chem 18:438–446

McQuade P, Miao Y, Yoo J, Quinn TP, Welch MJ, Lewis JS (2005) Imaging of melanoma using ^{64}Cu- and ^{86}Y-DOTA-ReC-CMSH(Arg^{11}), a cyclized peptide analogue of α-MSH. J Med Chem 48:2985–2992

Shi J, Wang L, Kim YS, Zhai S, Liu Z, Chen X, Liu S (2008) Improving tumor uptake and excretion kinetics of ^{99m}Tc-labeled cyclic arginine-glycine-aspartic (RGD) dimers with triglycine linkers. J Med Chem 51:7980–7990

Shi J, Wang L, Kim YS, Zhai S, Liu Z, Chen X, Liu S (2009) Improving tumor uptake and pharmacokinetics of ^{64}Cu-labeled cyclic RGD dimers with triglycine and PEG_4 linkers. Bioconj Chem 20:750–759

Smith-Jones PA, Vallabahajosula S, Goldsmith SJ, Navarro V, Hunter CJ, Bastidas D, Bander NH (2000) In vitro characterization of radiolabeled monoclonal antibodies specific for the extracellular domain of prostate specific membrane antigen. Cancer Res 60:5237–5243

Stimmel JB, Kull FC Jr (1998) Samarium-153 and lutetium-177 chelation properties of selected macrocyclic and cyclic ligands. Nucl Med Biol 25:117–125

Thumshirn G, Hersel U, Goodman SL, Kessler H (2003) Multimeric cyclic RGD peptides as potential tools for tumor targeting: solid-phase peptide synthesis and chemoselective oxime ligation. Chem Eur J 9:2717–2725

Wang L, Kim YS, Shi J, Zhai S, Jia B, Liu Z, Zhao H, Wang F, Chen X, Liu S (2009) Improving tumor targeting capability and pharmacokinetics of ^{99m}Tc-labeled cyclic RGD dimers with PEG_4 linkers. Mol Pharm 6:231–245

Weber WA, Haubner R, Vabuliene E, Kuhnast B, Webster HJ, Schwaiger M (2001) Tumor angiogenesis targeting using imaging agents. Q J Nucl Med 45:179–182

Wu Y, Zhang X, Xiong Z, Cheng Z, Fisher DR, Liu S, Gambhir SS, Chen X (2005) MicroPET imaging of glioma integrin $\alpha_v\beta_3$ expression using ^{64}Cu-labeled tetrameric RGD peptide. J Nucl Med 46:1707–1718

Wu Z, Li Z, Cai W, He L, Chin FT, Li F, Chen X (2007a) ^{18}F-labeled mini-PEG spacered RGD dimmer (^{18}FPRGD2): synthesis and micro-PET imaging $\alpha_v\beta_3$ integrin expression. Eur J Nucl Med Mol Imaging 34:1823–1831

Wu Z, Li Z, Chen K, Cai W, He L, Chin FT, Li F, Chen X (2007b) Micro-PET of tumor integrin $\alpha_v\beta_3$ expression using ^{18}F-labeled PEGylated tetrameric RGD peptide (^{18}F-FPRGD4). J Nucl Med 48:1536–1544